

Confined Multilamellae Prefer Cylindrical Morphology

Jung-Ren Huang*, Ling-Nan Zou, Thomas A. Witten

*James Franck Institute and Department of Physics, University of Chicago
5640 S. Ellis Avenue, Chicago, Illinois 60637, USA*

November 12, 2018

Abstract

By evaporating a drop of lipid dispersion we generate the myelin morphology often seen in dissolving surfactant powders. We explain these puzzling nonequilibrium structures using a geometric argument: The bilayer repeat spacing increases and thus the repulsion between bilayers decreases when a multilamellar disk is converted into a myelin without gain or loss of material and with number of bilayers unchanged. Sufficient reduction in bilayer repulsion can compensate for the cost in curvature energy, leading to a net stability of the myelin structure. A numerical estimate predicts the degree of dehydration required to favor myelin structures over flat lamellae.

1 Introduction

The phospholipid molecules that constitute the chief component of cellular plasma membranes spontaneously self-assemble to form bilayers when dissolved in water. These bilayers tend to stack to form multilayers, also known as *multilamellae*. At high lipid concentrations, the stable morphology consists of flat, stacked bilayers with quasi-long-range order [1, 2, 3]. Yet, under certain nonequilibrium conditions, the bilayers bend to form long-lived spherical multilamellae known as onions[4, 5] or nested cylindrical tubes called myelin figures or simply, myelins (see Fig.1)[5, 6, 7, 8, 9], despite the additional penalty in curvature energy. The formation of myelins has been a mystery since their discovery more than 150 years ago[6, 9]. Myelins offer a variety of potential applications such as encapsulation and controlled delivery of drugs[10]. Thus a better understanding of their formation and structure is desired.

In this paper we identify a type of constrained equilibrium that leads naturally to myelin formation. The simple geometrical mechanism proposed here offers a plausible and general explanation for the longstanding puzzle of myelin formation and has explicit implications about their internal makeup. We note that in contrast to the H_{II} -to- L_{α} -to- H_{II} reentrant phase transition[11] that involves topological changes, the formation of myelins in our system involves only geometrical changes.

This paper is organized as follows: In Section 2 we outline our experimental results of myelin formation. Based on the experimental observations, we propose a model in Sections 3 and 4 to explain the formation of myelins in our experiment. In Section 5 we investigate the effect of water permeation on our model. In Section 6 we discuss the implications and limitations of our model. Finally Section 7 concludes our work.

*email: jhuang2@uchicago.edu

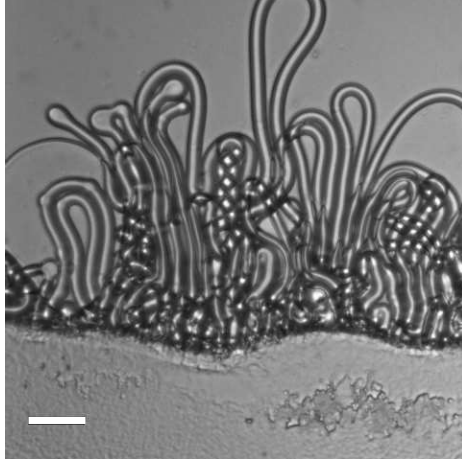


Figure 1: Formation of myelin figures in a typical contact experiment. A lump of concentrated dilauroyl phosphatidylcholine (DLPC) (bottom) is contacted with water (top) at 27°C. Closely packed myelins form at the interface and grow toward the water-rich side. The experimental approach has been described in detail in many references such as [5, 7, 8]. The bar at the lower left corner represents 100 μ m.

2 Experiment

The main goal of this paper is to present our model of myelin formation. Therefore we only summarize our experimental results that are pertinent to the model. More complete description of the experiment will be given elsewhere[12].

In our experiment we observe a drop of dilute suspension of dimyristoyl phosphatidylcholine (DMPC) bilayer vesicles in water as it evaporates[12] (Fig.2). The drop is heated to 27–30°C, above the chain-melting temperature of DMPC (\approx 24°C)[13]. Thus the bilayers are in the fluid state (L_α phase)[1]. The evaporative flow creates a ring deposit of concentrated lipid around the drop’s perimeter[14]. From this deposit many pancake-like multilamellar disks develop and grow inward. As the disks grow, they undergo a shape transition to form myelins. Experimental evidence suggests that materials, i.e., lipid and water enter the disk-myelin complex mainly via its root embedded in the dry deposit region (Fig.2)[5, 8]. If evaporation is halted, growth stops and the myelin is resorbed into its parent disk; but the myelin’s cylindrical morphology is retained during the resorption. This suggests that the disk-myelin complex is in quasi-equilibrium[15], and hence free energy analysis is applicable to the disk-to-myelin shape transition.

3 Model Definition

In this section and the next one, we present a theory to account for the myelin formation, i.e., the disk-to-myelin shape transition, observed in our experiment (Fig.2). We will show that the formation of myelins can be favorable because their cylindrical form results in a larger bilayer repeat spacing (i.e., separation between bilayers) and hence lower inter-bilayer repulsion than flat multilamellae.

We postulate that **(a)** the number of bilayers is unchanged during the shape transition, and **(b)** the bilayers can exchange materials, i.e., lipid and water, freely to achieve quasi-

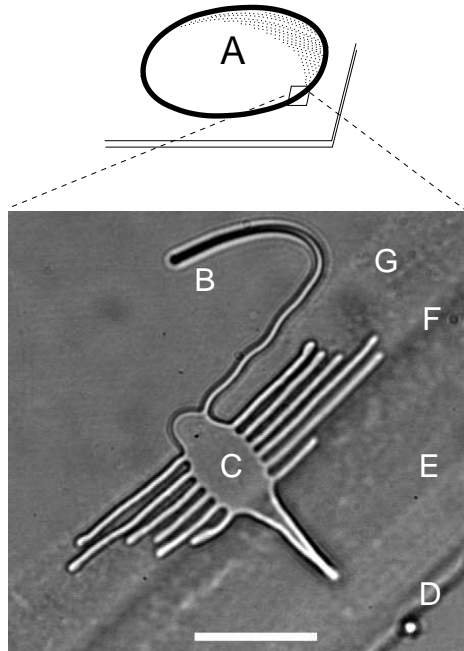


Figure 2: Optical micrograph of disk-myelin complex. Myelins emerge from a multilamellar disk at the perimeter of a water drop containing dilute dispersion of DMPC bilayer vesicles[12]. A: overview of the drop. B: myelin. C: multilamellar disk. D: initial contact line. E: dry DMPC deposit. F: current contact line. G: a band of aggregated vesicles. At the moment of the photo, only the long curved myelin was growing at about $0.5\mu\text{m/s}$. At later times, the long myelin drifted into place beside the straight myelins and another myelin pinched off from the tip of the disk, repeating the cycle. The bar at the bottom represents $20\mu\text{m}$.

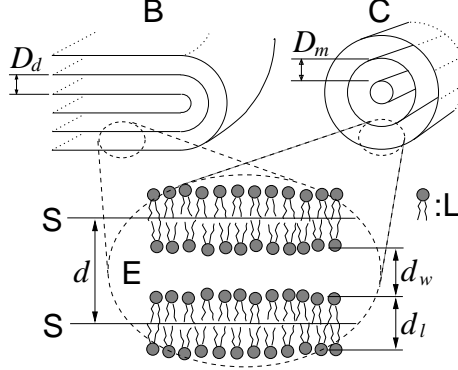


Figure 3: Cross-sectional view of a multilamellar disk (B) and a myelin (C). Both structures are composed of N uniformly spaced bilayers. Figure shows the special case of $N = 3$. Oval inset (E) shows placement of lipid molecules (L) making up bilayers. The symbol S represents the mid-surface of a bilayer. The total bilayer area A is measured at S. In this work we neglect the thermal undulations of bilayers (see Section 6)[23, 24]. Therefore A can be determined simply from the geometry of the disk or myelin. The bilayer repeat spacing D_d or $D_m = d = d_w + d_l$, where d_w is the water layer spacing and d_l the bilayer thickness. If the inter-bilayer pressure is sufficiently low, d_l is roughly constant and therefore the change in d is mostly due to that in d_w (Fig.1 of [20]).

equilibrium[15]. The number of bilayers, denoted by N , is unlikely to change on the time scale of the shape transition, which is about 1 second. The bilayers may exchange materials via defects such as screw dislocations[16, 17, 18].

The free energy includes a curvature energy favoring flat bilayers[19] and a repulsion between bilayers[20, 21, 22]. The curvature energy of a bilayer of area A takes the form of (Fig.3)

$$\frac{\kappa_c}{2} \int_A dA (c_1 + c_2 - c_0)^2, \quad (1)$$

where κ_c is the bending stiffness, c_1 and c_2 are the principal curvatures, and c_0 is the spontaneous curvature[19]. The bending stiffness

$$\kappa_c = 1.2 \times 10^{-19} \text{ J} \quad (2)$$

for DMPC bilayers[25]. (However, Ref.[26] gives a smaller value of κ_c .) In our experiment we expect $c_0 \simeq 0$. Postulate (a) implies that the topology of the disk-myelin complex does not change in the shape transition. Therefore we can neglect the Gaussian curvature contributions according to the Gauss-Bonnet theorem[27]. With (1) the curvature energy of a myelin consisting of N concentric, uniformly spaced bilayer cylinders is given by

$$\kappa_c \frac{\pi L}{D_m} \ln \left(\frac{R_o}{R_i} \right), \quad (3)$$

where L is the myelin length and D_m the bilayer repeat spacing (Fig.3); R_o and R_i are the radii of the outermost and innermost cylinders respectively. The total bilayer area

$$A = \pi N (R_i + R_o) L. \quad (4)$$

By construction

$$R_o = R_i + (N - 1)D_m. \quad (5)$$

In this paper we set (see Section 6)

$$R_i = \frac{D_m}{2} \quad (6)$$

for convenience, and we only consider myelins of large aspect ratios, i.e., $L \gg R_o$, so that the end caps are negligible.

The repulsion between bilayers is determined experimentally: The authors of [20] found that their pressure data were well represented as the sum of an exponentially falling hydration force plus a van der Waals attraction (Table 1 of [20]). Our estimates of inter-bilayer interaction energy use this functional form. Specifically, given water layer thickness d_w and bilayer repeat spacing d (Fig.3), the inter-bilayer pressure

$$P = P_1 + P_2, \quad (7)$$

where the hydration pressure

$$P_1(d_w) = P_0 \exp\left[-\frac{d_w}{\lambda}\right], \quad (8)$$

and the van der Waals attraction

$$P_2(d_w) = -\frac{H}{6\pi} \left[\frac{1}{d_w^3} - \frac{2}{d^3} + \frac{1}{(d + d_w)^3} \right]. \quad (9)$$

The inter-bilayer interaction energy per unit bilayer area is therefore equal to

$$-\int_{\infty}^{d_w} d(\tilde{d}_w) P(\tilde{d}_w). \quad (10)$$

In this paper the bilayer thickness d_l is taken to be constant (see Fig.3). The pressure $P_0 = 10^{9.94}$ dyne/cm² and $\lambda = 0.26$ nm for DMPC bilayers, and the Hamaker coefficient H is set to 10^{-20} J in this paper[20, 28]. When the bilayers are curved, this energy is in principle altered. In Section 6 we argue that such corrections are negligible in the case of interest.

Postulate (b) proposed at the beginning of the section implies that the important external parameters for determining the free energies are the amount of lipid and that of water in the disk-myelin complex. Under moderate external pressure, the bilayer thickness d_l is approximately constant and, moreover, both lipid bilayers and water are virtually incompressible (Fig.3)[20]. This means we can describe the amount of lipid by the total area A of all the bilayers, which is measured at the bilayer's mid-surface (S in Fig.3). Similarly, the total amount of lipid plus water is equivalent to the total volume V of the complex.

Given the total bilayer area A , volume V , and the number of bilayers N , the disk-myelin complex is internally confined. In this case the lipid concentration A/V determines the bilayer repeat spacing and thus the inter-bilayer repulsion, as shown in the next section.

4 Instability of the Disk

We now illustrate how a sufficiently large lipid concentration, i.e., area-to-volume ratio A/V , can make a multi-lamellar disk unstable to myelin formation.

We consider a large but thin disk composed of N nested bilayer disks, with uniform bilayer repeat spacing D_d , volume V , and total bilayer area A . Because the disk is large and thin,

its rim part is negligible. Figure 3 shows the example with $N = 3$. If the area of each bilayer is denoted by A_1 , then the total area $A = 2NA_1$ and the total volume $V = (2N - 1)D_dA_1$. Thus the repeat spacing

$$D_d = \left(1 + \frac{1}{2N - 1}\right) \frac{V}{A}. \quad (11)$$

This D_d determines the inter-bilayer interaction energy (see (10)). For these flat bilayers, the curvature energy (1) is arbitrarily small.

To show the instability of this disk, we convert it into a myelin composed of N concentric and uniformly spaced cylindrical bilayers, keeping both V and A fixed (Fig.3). Using (4), (5) and (6) the bilayer area $A = \pi LN^2 D_m$ while the myelin volume $V = \pi R_o^2 L = \pi L(N - 1/2)^2 D_m^2$. Thus $V/A = (1 - 1/2N)^2 D_m$ so that the myelin repeat spacing

$$\begin{aligned} D_m &= \left(1 + \frac{1}{2N - 1}\right)^2 \frac{V}{A} \\ &= \left(1 + \frac{1}{2N - 1}\right) D_d > D_d. \end{aligned} \quad (12)$$

This D_m determines the inter-bilayer interaction energy of the myelin (see (10)). With (5) and (6) its curvature energy (3) can be written as

$$\kappa_c \frac{\pi L}{D_m} \ln(2N - 1) \quad (13)$$

Because the myelin has a larger repeat spacing, it has a lower repulsion energy than the disk. If the decrease in the repulsion energy can compensate for the myelin's curvature energy (see (10) and (13)), the myelin, rather than the disk, becomes the thermodynamically more stable morphology. Here we define a threshold inter-bilayer pressure P_{th} , above which the disk becomes unstable against myelin formation. Namely, P_{th} is the pressure at which the decrease in the inter-bilayer repulsion energy due to the disk-to-myelin transition is equal to the curvature energy of the myelin.

Although the fractional change in spacing

$$\frac{D_m - D_d}{D_d} = \frac{1}{2N - 1} \approx \frac{1}{2N} \quad (14)$$

is tiny when $N \gg 1$, the reduction in the total repulsion energy is proportional to N , and therefore the effect of spacing increase can still be significant, as demonstrated by the example below.

Since the inter-bilayer pressure increases rapidly with decreased repeat spacing (7), a multilamellar disk with modest dehydration can easily have enough repulsion to become unstable. A typical disk observed in the experiment should be somewhat dehydrated because part of it is in the dry deposit region (Fig.2). The disk thickness is observed to be about 2.5 μm [12]. Given the equilibrium spacing[20], we infer the number N of nested bilayer disks to be approximately 200.

Taking $N = 200$ and using the measured bending stiffness (2) and inter-bilayer repulsion (7) for these DMPC bilayers[20], our model predicts that the energy of the disk becomes larger than that of the myelin when the dehydration exceeds 2.1%, i.e., a 2.1% decrease in the repeat spacing from the equilibrium value of 6.22nm[20]. The inter-bilayer pressure $P = P_{th} \approx 0.32\text{atm}$ at such dehydration (7). The myelin converted from this disk has a repeat spacing about 1.9% less than the equilibrium value and an inter-bilayer pressure P of about

0.3atm, with the van der Waals attraction $P_2 \simeq 0.013\text{atm}$ (9). Since the difference between the repeat spacings, D_d and D_m , is tiny, the myelin diameter is nearly identical with the thickness of the parent disk; this is consistent with our experimental observations[12]. Here we assume that the threshold pressure P_{th} is sufficiently low so that the bilayer thickness d_l is unchanged during the shape transformation (Fig.3). With the experimental data shown in Fig.1 of [20], our result of $P_{th} \approx 0.32\text{atm}$ suggests that a constant d_l is indeed a fair approximation.

Based on our model we propose the following scenario to explain the myelin formation in our experiment (Fig.2): As water evaporates, lipid and water enter the disk, and hence both A and V increase. Because the contact line gradually moves inward due to water evaporation, the disk becomes more and more dehydrated, i.e., the lipid concentration A/V increases. An increase in A/V leads to a decrease in the repeat spacing D_d (11) and thus an increase in the inter-bilayer repulsion (7). The repeat spacing keeps decreasing until a threshold, below which the disk is unstable and a myelin with a larger spacing grows out of it in order to lower the free energy.

5 Effect of Water Permeation

The above simple example has a large pressure difference $\approx 0.3\text{atm}$ between the inside and outside of the disk-myelin complex. This pressure might induce sufficient water permeation through the bilayers to reduce the dehydration and restore the stability of the disk morphology, thus invalidating our model. In the following we perform a self-consistency check to show this is not the case: In practice the system should be in a steady state, where the pressure drop occurs across a significant fraction of the complex. This suggests that the pressure difference across a bilayer in the complex of Figure 2 is about $1\text{atm}/N \approx 1\text{atm}/200 = 5 \times 10^{-3}\text{atm}$. The water permeability coefficients p_w for typical phosphatidylcholine bilayers are known to be 30-100 $\mu\text{m}/\text{s}$ [29]. Assuming the validity of the solubility-diffusion mechanism[30], the volume flux of water across a bilayer of area A_2 is given by

$$J_v = p_w \frac{\bar{V}_w A_2}{RT} \Delta P,$$

where ΔP is the pressure difference across the bilayer, $\bar{V}_w = 18\text{cm}^3/\text{mole}$, the partial molar volume of water, R the gas constant and T the temperature. Using permeability coefficient $p_w = 100\mu\text{m}/\text{s}$ and assuming that water enters the complex only via permeation and spreads evenly into all water layers, we estimate that permeation causes each water layer to swell at the rate of $\dot{d}_w \approx 2 \times 10^{-3}\text{nm}/\text{s}$, or equivalently, 1.8% of the equilibrium spacing per minute (Fig.3). Given the disk diameter = $15\mu\text{m}$ and the swelling rate \dot{d}_w , the flux of water permeating into the disk part of the complex is

$$J_d \approx 0.06\mu\text{m}^3/\text{s},$$

which only accounts for a small portion of the total water influx

$$J_T \approx 1\mu\text{m}^3/\text{s}$$

inferred from the observed myelin growth rate $\approx 0.5\mu\text{m}/\text{s}$ (Fig.2). The growth of myelins implies that both the bilayer area A and volume V of the complex increase with time. Our model, nevertheless, requires that the concentration A/V is maintained at a sufficiently high

level so that the disk is always unstable against the formation of myelins. Since $J_d \ll J_T$, the effect of water permeation is too weak to cause any significant decrease in A/V and thus to compromise the proposed mechanism for myelin formation. By the same token, the flux of water permeating into a myelin in Figure 2 is given by

$$J_m \approx 2.9 \times 10^{-3} L \mu\text{m}^3/\text{s},$$

where the myelin length L is in μm and the myelin diameter is set to $2.5\mu\text{m}$. Now we can define a critical myelin length L_c using the equation

$$J_T = J_d + J_m(L_c).$$

When the myelin length $L > L_c$, our mechanism for myelin formation no longer holds because the flux due to water permeation, $J_d + J_m$ exceeds the total influx J_T and thus the concentration A/V must decrease, restoring the stability of the disk morphology. Given J_T , J_d and J_m calculated above, L_c is about $320\mu\text{m}$. In Figure 2 the lengths of all the myelins are less than L_c , which means our model for myelin formation can be applied to this system with self-consistency.

6 Discussion

The model presented in Sections 3 and 4 offers a simple geometrical explanation for the formation of myelins in our experiment: The bilayer repeat spacing increases and therefore the inter-bilayer repulsion decreases when a multilamellar disk is transformed into a myelin under the constraints of fixed volume, bilayer area, and number of bilayers (see (11) and (12)). If the lipid concentration is sufficiently high, the decrease in the inter-bilayer repulsion energy is greater than the curvature energy of the myelin, and thus the disk is unstable against myelin formation. Our model can be thought of as a minimal model for myelin formation, from which more sophisticated models can be constructed. For systems with non-negligible disk perimeter and myelin end-caps, the proposed geometrical mechanism still holds, but the expressions for D_d and D_m are no longer as simple as (11) and (12), respectively[31]. In the following we will discuss the limitations as well as the implications of our model.

In Section 3 we impose two artificial (i.e., non-physical) constraints on the myelin geometry in order to illustrate the geometrical mechanism that destabilizes the disk: The constituent bilayer cylinders of a myelin are uniformly spaced, and the radius $R_i = D_m/2$ (equation (6)). With these two constraints the calculations of the energies (3) and (10) are greatly simplified. Freeing these two constraints would not weaken our proposed mechanism for myelin formation in that allowing D_m to be non-uniform or R_i to vary can only lower the myelin energy further. We will investigate the myelin structure without these two constraints in another work[31].

In our model we neglect the thermal undulations of bilayers[23, 24] (Fig.3). The reasons are twofold: First, the persistence length[32, 33] of DMPC bilayers is much larger than any lengths of the disk-myelin complexes observed in our experiment (Fig.2). This means the bilayers are stiff, and thus their undulations should be negligible. Secondly, although bilayer thermal undulations decrease the bending stiffness κ_c (2)[33, 34, 35] and increase the inter-bilayer pressure P (7)¹, these effects, however, would only help destabilize the disk and therefore would not invalidate our model. Moreover, the threshold pressure P_{th}

¹The thermal undulations of bilayers alter the functional form of the hydration pressure P_1 (8)[28, 36].

defined in Section 4 is insensitive to bilayer undulations, as shown below: The decrease in the inter-bilayer repulsion energy due to the disk-to-myelin transition can be approximated with $P_{th}A(D_m - D_d) = P_{th}AD_d/(2N - 1)$ (see (10) and (14)). By definition P_{th} satisfies (see (3)–(6), and (12))

$$\begin{aligned} P_{th} \frac{AD_d}{2N - 1} &\approx \kappa_c \frac{\pi L}{D_m} \ln \left(\frac{R_o}{R_i} \right) \\ &= \kappa_c \frac{A(N - 1/2)^2 \ln(2N - 1)}{D_d^2 \cdot N^3(N + 1/2)}. \end{aligned} \quad (15)$$

Using $N = 200$ and equation (2), and assuming D_d is about equal to the equilibrium value of 6.22nm for DMPC bilayers (Section 4), the above equation yields the threshold pressure $P_{th} \approx 0.3\text{atm}$ regardless of bilayer undulations. This estimate of P_{th} is close to the result, 0.32atm, obtained in Section 4. In the above calculation we neglect the weak dependence of κ_c on bilayer undulations[33, 34, 35].

Based on the experimental evidence described in Section 2, we postulate that the bilayers can exchange materials through defects to reach quasi-equilibrium (postulate (b) in Section 3). This postulate is important in our model in that it greatly simplifies the problem. Therefore the formation of defects in systems like ours deserve more detailed investigation[16, 17, 18].

Our theory says nothing about how the myelin size is determined. This size appears to be determined by pre-existing structure in the dry lipid from which the disk and myelins grow (Fig.2). However, our theory does suggest consequences of changes in size: Since the bilayer repeat spacing is of the order of the equilibrium spacing, the overall diameter of the myelin tube is proportional to the number of bilayers N . We see from equation (15) that the threshold pressure P_{th} is proportional to $\ln N/N$ for large N . Thus an increase in the myelin diameter should produce a roughly proportionate decrease in the internal pressure.

Our analysis of inter-bilayer interaction energy assumes that the bilayers are flat. However, in the myelin structure the bilayers are curved. This in principle induces a correction to the interaction energy per unit area (10). In the following we show that this correction is negligible when the number of bilayers $N \gg 1$: Equations (4)–(6), (8) and (14) imply that the net change of the interaction energy due to the spacing increase is approximately

$$P_1 A(D_m - D_d) \simeq \frac{\pi}{2} L D_m^2 P_1 N \sim N. \quad (16)$$

Using equation (8) the interaction energy density (10) of two adjacent bilayer cylinders of radii $\simeq R$ in a myelin is about

$$P_1 \lambda \left[1 + c \left(\frac{D_m}{R} \right)^2 \right], \quad (17)$$

where the dimensionless prefactor c is expected to be of order 1. The correction term $c(D_m/R)^2$ results from the bilayer curvature $1/R$. Terms of order $(D_m/R)^1$ would depend on the direction of curvature, and are thus ruled out by symmetry. With (5), (6) and (17) the correction to the inter-bilayer interaction energy of a myelin due to nonzero bilayer curvatures is given by

$$\begin{aligned} cP_1 \lambda \sum_{n=1}^N A_n \left(\frac{D_m}{R_n} \right)^2 &\simeq 2\pi c P_1 \lambda D_m L \ln(2N) \\ &\sim \ln(2N), \end{aligned} \quad (18)$$

where the decay length $\lambda < D_m$ (8), and $R_n = R_i + (n - 1)D_m$ and $A_n = 2\pi R_n L$ are the radius and area of the n -th bilayer cylinder of the myelin, respectively. The above estimates suggest that the curvature effect (18) is negligible compared to our main effect (16) when $N \gg 1$.

In Section 4 we show that the repeat spacing increases when an N -bilayer disk is transformed into an N -bilayer myelin (see (11) and (12)). The spacing would increase further if the myelin were converted into concentric spheres or onions[4] also composed of N uniformly spaced bilayers. Specifically, the onion spacing $\simeq (1 + 1/(2N - 1))D_m > D_m$ for $N \gg 1$. This suggests that our model might help understand the formation of onions observed in [4] and [5]. In our experiment (Fig.2) their formation is, however, kinetically blocked because they cannot form continuously from a disk or myelin. Furthermore, the relative stability of onions is also influenced by the Gaussian bending stiffness[19], since the transformation from a disk or myelin to onions changes the topology[27].

Although our model is invented mainly to account for the disk-to-myelin transition shown in Fig.2, it also sheds some light on the formation of myelins observed in contact experiments (see Fig.1)[5, 7, 8]: In a contact experiment water is brought into contact with concentrated surfactant. Immediately after contact, the surfactant molecules self-organize to form many multilamellae at the interface[18]. These multilamellae should have high lipid concentrations, and therefore their inter-bilayer interaction is strongly repulsive. As a result, the bilayers along the contact interface would curve to form myelinic structures.

7 Conclusions

In this paper we propose a geometrical mechanism to account for the formation of myelins: In short, if a stack of flat bilayers is internally confined and the inter-bilayer interaction is repulsive, geometrical packing alone can lead to myelin formation. We believe this geometric mechanism can help explain why myelins form in a variety of experiments[5, 7, 8], where internal confinement and inter-bilayer repulsion also appear to play important roles. Our findings may help develop techniques in controlled growth of myelin or onion structures, which have potential applications in encapsulation and drug delivery[10]. We emphasize that our model, by its very nature, addresses only the equilibrium aspect of myelin formation. Many questions such as the myelin size distribution and the myelin growth rate still await answers.

Acknowledgements

We would like to thank Prof. de Gennes and Prof. Kozlov for useful discussions. This work was supported in part by the MRSEC Program of the National Science Foundation under Award Number DMR-0213745. L.-N. Zou was partially supported by a GAANN fellowship from the U.S. Department of Education.

References

- [1] R.G. Laughlin, *The Aqueous Phase Behavior of Surfactants* (Academic Press, San Diego, 1996)
- [2] D. Roux, C.R. Safinya, F. Nallet, in *Micelles, Membranes, Microemulsions, and Monolayers*, edited by W.M. Gelbart, A. Ben-Shaul, D. Roux (Springer, New York, 1994)

- [3] P.G. De Gennes, J. Prost, *The Physics of Liquid Crystals*, 2nd edn. (Oxford University Press, New York, 1993)
- [4] O. Diat, D. Roux, F. Nallet, *J. Phys. II France* **3**, 1427 (1993)
- [5] M. Buchanan, S.U. Egelhaaf, M.E. Cates, *Langmuir* **16**, 3718 (2000)
- [6] R. Virchow, *Virchow's Arch.* **6**, 562 (1854)
- [7] I. Sakurai, T. Suzuki, S. Sakurai, *Mol. Cryst. Liq. Cryst.* **180B**, 305 (1990)
- [8] M. Haran, A. Chowdhury, C. Manohar, J. Bellare, *Colloids Surf. A* **205**, 21 (2002)
- [9] M. Buchanan, in *Nonlinear Dynamics in Polymeric Systems*, edited by J.A.Pojman, Q. Tran-Cong-Miyata (American Chemical Society, Washington, DC, 2004)
- [10] D.D. Lasic, *Liposomes: From Physics to Applications* (Elsevier, Amsterdam, 1993).
- [11] M.M. Kozlov, S. Leikin, R.P. Rand, *Biophys. J.* **67**, 1603 (1994)
- [12] L.-N. Zou, S.R. Nagel (unpublished)
- [13] S. Mabrey, J.M. Sturtevant, *Proc. Natl. Acad. Sci. USA* **73**, 3862 (1976)
- [14] R.D. Deegan et al., *Nature* **389**, 827 (1997); *Phys. Rev. E* **62**, 756 (2000)
- [15] P.B. Warren, M. Buchanan, *Curr. Opin. Colloid Interface Sci.* **6**, 287 (2001)
- [16] M. Kléman, *Points, Lines and Walls: In Liquid Crystals, Magnetic Systems and Various Ordered Media* (John Wiley & Sons, New York, 1983)
- [17] W.J. Benton, K.H. Raney, C.A. Miller, *J. Colloid Interface Sci.* **110**, 363 (1986)
- [18] A. Sein, J.B.F.N. Engberts, *Langmuir* **12**, 2924 (1996)
- [19] T.A. Witten, *Structured Fluids: Polymers, Colloids, Surfactants* (Oxford University Press, New York, 2004)
- [20] L.J. Lis et al., *Biophys. J.* **37**, 657 (1982)
- [21] J.N. Israelachvili, H. Wennerström, *J. Phys. Chem.* **96**, 520 (1992)
- [22] J.N. Israelachvili, *Intermolecular and Surface Forces*, 2nd edn. (Academic Press, San Diego, 1998)
- [23] W. Helfrich, *Z. Naturforsch.* **33a**, 305 (1978)
- [24] W. Helfrich, R.-M. Servuss, *Nuovo Cimento D* **3**, 137 (1984)
- [25] W. Häckl, U. Seifert, E. Sackmann, *J. Phys. II France* **7**, 1141 (1997)
- [26] G. Pabst, J. Katsaras, V.A. Raghunathan, M. Rappolt, *Langmuir* **19**, 1716 (2003)
- [27] D.J. Struik, *Lectures on Classical Differential Geometry*, 2nd edn. (Dover, New York, 1988).
- [28] E.A. Evans, V.A. Parsegian, *Proc. Natl. Acad. Sci. USA* **83**, 7132 (1986)

- [29] S.-J. Marrink, H.J.C. Berendsen, *J. Phys. Chem.* **98**, 4155 (1994)
- [30] A. Finkelstein, *Water Movement Through Lipid Bilayers, Pores, and Plasma Membranes: Theory and Reality* (John Wiley & Sons, New York, 1987)
- [31] J.-R. Huang, T.A. Witten (unpublished)
- [32] P.G. De Gennes, C. Taupin, *J. Phys. Chem.* **86**, 2294 (1982)
- [33] D. Sornette, N. Ostrowsky, in *Micelles, Membranes, Microemulsions, and Monolayers*, edited by W.M. Gelbart, A. Ben-Shaul, D. Roux (Springer, New York, 1994)
- [34] L. Peliti, S. Leibler, *Phys. Rev. Lett.* **54**, 1690 (1985)
- [35] W. Helfrich, *J. Phys. Paris* **46**, 1263 (1985)
- [36] R.P. Rand, V.A. Parsegian, *Biochim. Biophys. Acta* **988**, 351 (1989)